nature catalysis

ARTICLES

https://doi.org/10.1038/s41929-021-00688-w

Check for updates

Cobalt-catalysed enantioselective C(sp^3)–C(sp^3) coupling

Yan Li[1,3], Wan Nie[1,3], Zhe Chang[1,3], Jia-Wang Wang[1,3], Xi Lu[1]✉ and Yao Fu[1,2]✉

Enantioselective C(sp^3)–C(sp^3) coupling substantially impacts organic synthesis but remains challenging. Cobalt has played an important role in the development of homogeneous organometallic catalysis, but there are few examples of its use in asymmetric cross-coupling. Here we report a cobalt-catalysed enantioselective C(sp^3)–C(sp^3) coupling reaction, namely, alkene hydroalkylation, to access chiral fluoroalkanes. This reaction represents a catalyst-controlled enantioselective coupling mode in which a tailor-made auxiliary is unnecessary; via this reaction, an aliphatic C–F stereogenic centre can be introduced at the desired position in an alkyl chain.

Alkyl–alkyl bonds are pervasive among organic molecules, and the reliable generation of such bonds has a substantial impact on the retrosynthetic analysis and subsequent synthesis of molecules used in many disciplines[1]. A recent viewpoint also suggests that an increased number of stereogenic centres will be instrumental in the clinical success of a candidate drug molecule. Furthermore, effective tools are required for alkyl–alkyl bond formation with stereoselective processes[2,3]. However, enantioselective construction of an alkyl–alkyl bond remains challenging.

Transition-metal-catalysed electrophile–nucleophile cross-coupling has long been known as a powerful strategy to achieve enantioselective C(sp^3)–C(sp^3) bond formation[4,5]. The enantioenriched products can be accessed through a radical pathway activation of racemic alkyl electrophiles followed by enantioselective oxidation addition or reductive elimination (Fig. 1a)[6–8]. Fu and others have made significant progress in this area[4–8]. However, it is also universally acknowledged that the presence of a suitably positioned and conspicuous auxiliary group, which might interact with the catalyst in a stereo-determining step, has generally been necessary to achieve high enantioselectivities[9,10]. Various auxiliary groups have proven to be very effective, and as summed up by Fu and co-workers[9], the substrate needs to bear a Lewis alkaline heteroatom-directing group[11,12] (typically, oxygen or nitrogen in a carbonyl group or an aniline) or a proximal p/π orbital[13,14] (typically, a conjugated aryl, carbonyl or boryl group). Nickel-hydride-catalysed alkene hydrofunctionalization enables enantioselective C(sp^3)–C(sp^3) formation from readily available starting materials, obviates the need for prepreparation of hyperactive organometallic reagents and improves the functional group compatibility[15–17]. However, these reactions also conform to the previous rule that a proximal double bond is required for high enantioselectivity[18–20].

An alternative strategy to construct a chiral C(sp^3) centre involves metal hydride insertion across alkenes to generate organometallic species and allow enantiospecific or enantioselective cross-coupling (Fig. 1b). Copper-hydride-catalysed enantioselective hydrofunctionalization of internal alkenes is a good example, especially the asymmetric hydroamination to produce chiral amines[21,22]. Copper-hydride-catalysed hydroalkylation has been limited to activated alkyl halides (for example, allyl electrophiles) or intramolecular reactions[23,24]. Very recently, nickel hydride catalysis proved to be perfectly competent in this enantioselective catalytic mode. Nevertheless, it is clear that an ingeniously designed directing group (oxygen in a carbonyl group, or a conjugated boryl group) is necessary to form a stabilized alkylnickel intermediate and is vital to the hydrometalation step[25–30]. Therefore, the requirement for a suitable auxiliary group remains the decisive factor in stereochemical control.

On the other hand, cobalt exhibits advantages, such as low cost and toxicity, and has played an important role in the development of homogeneous organometallic catalysis[31]. Although cobalt catalysts have already proven to be highly efficient for carbon–carbon bond formation[32–34], cobalt is not well suited to the asymmetric version of the reaction[35–37]. In this article we establish a cobalt hydride catalytic system to achieve alkene hydroalkylation with a high level of regio- and enantioselectivity (Fig. 1c). We demonstrate that with the help of this robust and mild cobalt hydride catalytic system, we can successfully achieve enantioselective C(sp^3)–C(sp^3) coupling with substrates lacking common auxiliary group features. In addition, an aliphatic C–F stereogenic centre at the desired position in an alkyl chain can be rapidly introduced using readily available achiral fluoroalkenes and alkyl halides.

Results

Initial considerations. Because of its unique ability to enhance biological and physical properties, including the dipole moment, metabolic stability and target-binding affinity, the incorporation of fluorine atoms or fluorine-containing fragments has found a wide range of important uses in medicinal, agrochemical and material sciences applications[38,39]. Most techniques to achieve a stereogenic centre bearing a fluorine substituent involve enantiospecific transformation of functional groups or enantioselective fluorination adjacent to functional groups[40–47].

Reaction discovery and optimization. We commenced our study by evaluating the hydroalkylation of **1a**—readily synthesized on the scale of tens of grammes from aldehyde feedstock—with alkyl

[1]Hefei National Laboratory for Physical Sciences at the Microscale, CAS Key Laboratory of Urban Pollutant Conversion, Anhui Province Key Laboratory of Biomass Clean Energy, Center for Excellence in Molecular Synthesis of CAS, University of Science and Technology of China, Hefei, China. [2]Institute of Energy, Hefei Comprehensive National Science Center, Hefei, China. [3]These authors contributed equally: Y. Li, W. Nie, Z. Chang, J.-W. Wang. ✉e-mail: luxi@mail.ustc.edu.cn; fuyao@ustc.edu.cn

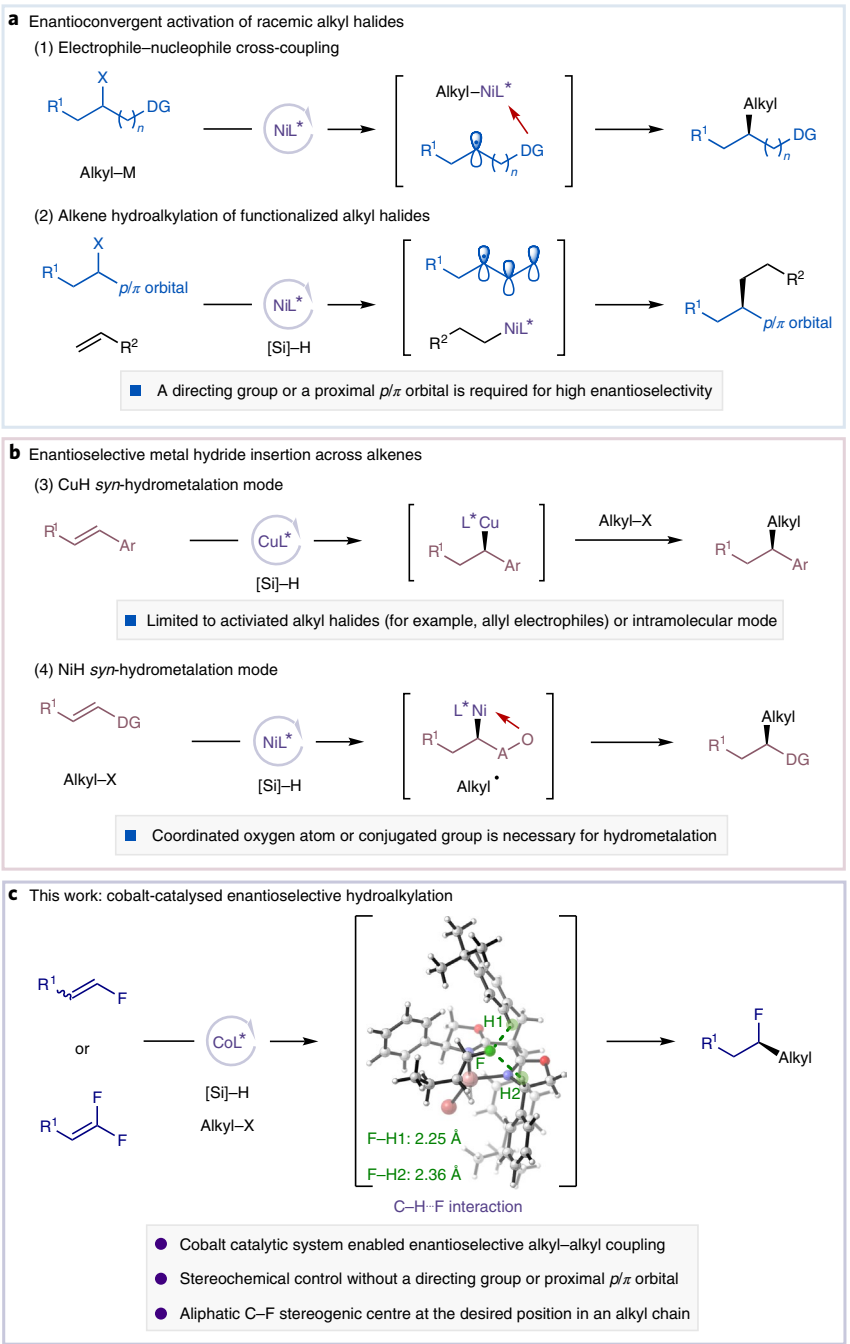

Fig. 1 | Transition-metal-hydride-catalysed enantioselective C(sp^3)–C(sp^3) coupling and our strategy. a, Nickel-catalysed enantioselective electrophile–nucleophile cross-coupling and alkene hydroalkylation. **b**, Copper- and nickel-catalysed enantioselective alkene hydroalkylation. **c**, Our strategy: cobalt-catalysed enantioselective alkene hydroalkylation. X, halide; DG, directing group; M, metal; **L***, chiral ligand; Ar, aryl; A, any linked atom.

iodide **2a** under reductive conditions to access chiral fluoroalkanes (Table 1). After systematic screening of all reaction parameters, a combination of $CoBr_2$(DME) and (*S*,*S*)-**L*** with DEMS and CsF in DME was found to be critical for success (entry 1), delivering fluoroalkene **4aa** with a 90% NMR yield, an 85% isolated yield and an excellent enantioselectivity profile (97% enantiomeric excess (e.e.)). A detailed comparison of the changes in each reaction parameter is summarized in Table 1 (see Supplementary Table 1 for more details). The structurally related bioxazoline **L1**, pyridine–bisoxazoline **L2** and pyridine–oxazoline **L3** ligands were inefficient (entry 2). A considerably improved yield of 37% and e.e. of 91% were obtained using the bisoxazoline ligand **L4** (entry 3). The increased steric hindrance on the 5-position substitution of the oxazoline ring would further improve the yield and enantioselectivity (entries 3 and 4, **L*** versus **L5** versus **L4**). Other cobalt sources were also tested, and many Co(II) salts could be used except $Co(acac)_2$ (entries 5–7). Additionally, Co(III) and Co(I) salts were invalid for this transformation (entry 8). In addition, the reaction could not be conducted in the absence of cobalt catalysts or through the use of copper, nickel or palladium catalysts. Oxygen-bearing silanes, such as PMHS, could be used (entry 9), but $MeEt_2SiH$ provided no product (entry 10). A moderately strong base, including KF

Table 1 | Optimization of the reaction conditions

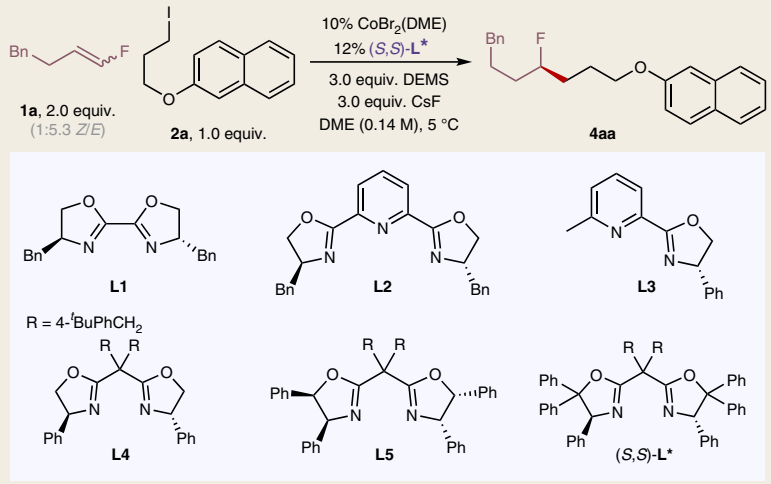

Entry	Variants	Yield (%)	e.e. (%)
1	None	90 (85)[a]	97
2	**L1**, **L2** or **L3**	Trace	-
3	**L4**	37	91
4	**L5**	52	91
5	$CoCl_2$	64	96
6	CoI_2	35	96
7	$Co(acac)_2$	Trace	-
8	$CoCl(PPh_3)_3$ or CoF_3	Trace	-
9	PMHS	71	97
10	$MeEt_2SiH$	Trace	-
11	Cs_2CO_3	40	98
12	KF	76	98
13	LiO^tBu	17	85
14	1,4-Dioxane[b]	23	91
15	Diglyme	86	96
16	DMAc	8	59
17	CH_3CN, DCE or $^iPr_2O$	Trace	-

Reactions were carried out under an argon atmosphere. Conditions: **1a** (2.0 equiv.), **2a** (1.0 equiv.), cobalt catalyst (10 mol %), ligand **L*** and **L1**-**L5** (12 mol%), silane (3.0 equiv.), base (3.0 equiv.), solvent (0.14 M), 5 °C, 12 h. 0.1 mmol scale. ^{19}F NMR yield. Benzotrifluoride was used as an internal standard. The e.e. value was determined by high-performance liquid chromatography (HPLC). DME, 1,2-dimethoxyethane; DMAc, *N*,*N*-dimethylacetamide; DCE, 1,2-dichloroethane; diglyme, bis(2-methoxyethyl) ether; DEMS, diethoxymethylsilane; PMHS, polymethylhydrosiloxane; acac, acetylacetone. [a]Isolated yield in parentheses. [b]15 °C.

and Cs_2CO_3, could provide satisfactory results (entries 11 and 12); however, lower yield was obtained using LiO^tBu (entry 13). Many other solvents were compared with the best, DME. For example, ethylene-glycol-derived ether solvents (entries 14 and 15), such as 1,4-dioxane and diglyme, afforded uniformly high enantioselectivity with yields of 23% and 86%, respectively. However, lower-polarity solvents (for example, DCE and $^iPr_2O$) exhibited extremely reduced conversion, while higher-polarity solvents (for example, DMAc and CH_3CN) were inferior due to significant hydrodehalogenation side reactions (entries 16 and 17).

Substrate scope of hydroalkylation. We investigated the preparative scope of this enantioselective coupling protocol (Figs. 2 and 3). As evident from the results summarized in Fig. 2, this reaction was widely applicable for a broad range of alkyl halides, including both alkyl iodides and bromides, producing satisfactory coupling efficiency (40–90% isolated yield) and enantioinduction (88–99% e.e.) in all cases. Note, however, that alkyl iodides generally provided better yields for the corresponding hydroalkylation products. Alkyl halides containing an ether (**4aa**, **4ab**), aryl ester (**4ac**), alkyl ester (**4ad**), trifluoromethyl (**4ae**), carbamate (**4ah**, **4ai**) and keto carbonyl (**4aj**) group were all favourably converted to the designated products, illustrating the excellent chemoselectivity profile of this reaction. Heterocycles containing sulfur (**4af**), oxygen (**4ag**, **4an**) and nitrogen (**4ah**) posed no problems. The presence of heteroatoms would not interfere with bisoxazoline ligands for binding to the catalyst centre. Additionally, the presence of alkyl and aryl chlorides (**4ak**, **4al**) and aryl bromide (**4km**) was perfectly compatible with producing $C(sp^3)$–$C(sp^3)$ bonds, offering the opportunity for further manipulations on the surviving electrophilic sites via conventional transformations. Methylation is widely used to fine-tune the biological activity and physicochemical properties of medicinal candidates in drug design. Interestingly, methylated products and their perdeuterated forms (**4ao**, **4lp**) were easily within reach through the reaction of iodomethane (**2o**) and trideuterioiodomethane (**2p**) with the corresponding fluoroalkene. In addition,

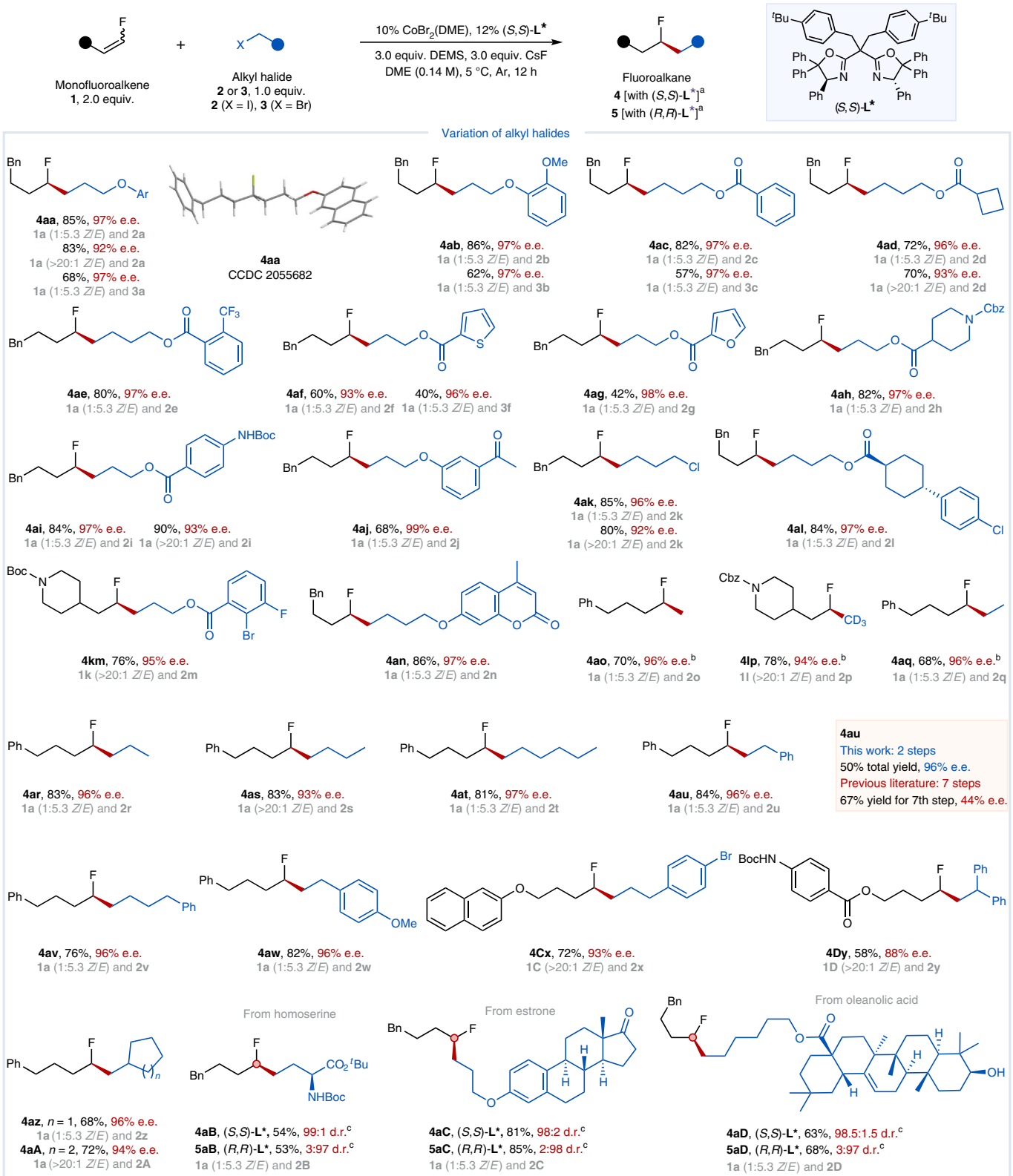

Fig. 2 | Scope of alkyl halides in hydroalkylation. [a]Standard conditions as shown in Table 1 (0.2 mmol scale; isolated yield). [b]Fluoroalkene **1** (1.0 equiv.) and alkyl iodide **2** (2.0 equiv.) were used. [c]Diastereocentres are marked with a spherical symbol. d.r. and e.e. values were determined by HPLC or supercritical fluid chromatography (SFC). Bn, benzyl; Ar, 2-naphthyl; Cbz, carbobenzyloxy; Boc, *t*-butoxycarbonyl; d.r., diastereomeric ratio.

many substrates (**4aq**, **4ar**, **4as**, **4at**, **4au**, **4av**, **4aw**, **4Cx**, **4Dy**, **4az** and **4aA**) strongly demonstrated that this reaction could enable coupling with alkyl halides lacking any heteroatom directing groups with high enantioselectivity. The substrate **4au**, which contains two highly similar alkyl substituents, was challenging to access and previously required a seven-step synthesis with 44% e.e.[42]. We were

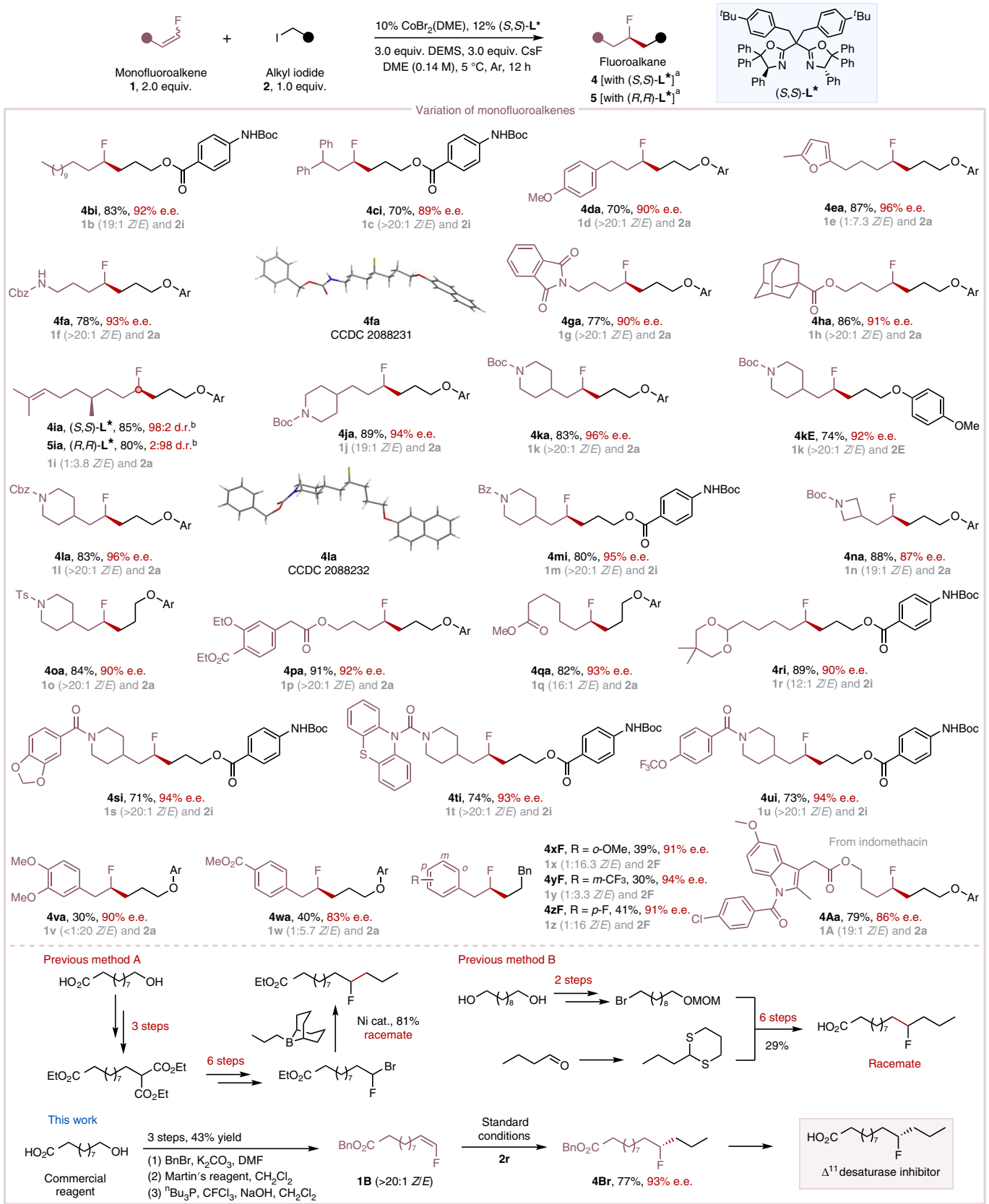

Fig. 3 | Scope of monofluoroalkenes in hydroalkylation. [a]Standard conditions as shown in Table 1 (0.2 mmol scale; isolated yield). [b]Diastereocentres are marked with a spherical symbol. d.r. and e.e. values were determined by HPLC or SFC. Ar, 2-naphthyl; Bz, benzoyl; Ts, tosyl; Martin's reagent, 1,1-dihydro-1,1,1-triacetoxy-1,2-benzoiodooxol-3(1*H*)-one; MOMO, methoxymethyl.

delighted to find that **4au** could be accessed in two steps with 50% total yield and 96% e.e. through our alkene hydroalkylation method.

Encouraged by these results, we focused our attention on studying the practicability of our protocol for the late-stage modification of drug molecules and natural products. An array of enantioenriched fluoroalkanes bearing structurally complicated or bioactive alkyl fragments could be synthesized successfully. For example, alkyl iodides derived from natural products such as homoserine (**4aB**, **5aB**), estrone (**4aC**, **5aC**) and oleanolic acid (**4aD**, **5aD**) were easily converted to potentially valuable products. Notably, the diastereomeric ratio at the bond forming the α-fluorine carbon centre was entirely determined by selecting the corresponding enantiomers of the ligand.

The hydroalkylation event occurred with equal ease for a host of monofluoroalkenes bearing various functional groups (Fig. 3). The monofluoroalkenes underwent targeted hydroalkylation to deliver the corresponding products regardless of whether the *Z* or *E* configuration of the starting monofluoroalkenes was utilized. Substrates containing Lewis alkaline heteroatoms (nitrogen, oxygen or sulfur) or coordinating groups (such as phthalimide, ester or aryl rings) located in various positions were all ideally used to produce targeted fluoroalkanes with high coupling efficiencies and excellent enantioselectivities. A notable example was the convenient synthesis of **4bi**, which demonstrated that the regio- and enantioselectivity was governed by the catalyst rather than the coordinating group in substrates. A high level of functional group compatibility was achieved, benefiting from both the mild cobalt-catalysed reaction conditions and the straightforward synthesis of monofluoroalkene raw materials via one-step Wittig olefination from aldehydes or olefin metathesis[48,49]. A broad set of synthetically valuable functional groups, which included aryl groups (**4ci**), methoxy arenes (**4da**), furans (**4ea**), carbamates (**4fa**), phthalimides (**4ga**), sulfonamides (**4oa**), esters (**4ha**, **4pa**, **4qa**), internal alkene double bonds (**4ia**, **5ia**), acetals (**4ri**, **4si**) and many medicinally relevant heterocycles, such as piperidines (**4ja**, **4ka**, **4kE**, **4la**, **4mi**, **4ti** and **4ui**) and azetidines (**4na**), were all well accommodated. We also examined the usability of this reaction with aromatic substituted monofluoroalkenes (**4va**, **4wa**, **4xF**, **4yF** and **4zF**). One limitation at the current stage was the moderate coupling yields and electronically relevant enantioselectivities. In terms of the trends, an electron-deficient substrate (**4wa**) generally provided a slightly diminished enantioselectivity. The monofluoroalkene **1A** derived from the drug molecule indomethacin readily delivered the desired product **4Aa**. Our alkene hydroalkylation method could be used in the synthesis of biochemically valuable compounds. Monofluoro myristic acid exhibits Δ^{11} desaturase inhibitory activity[50,51]. We can prepare the intermediate **4Br** for the concise synthesis of monofluoro myristic acid.

Finally, the absolute configuration of the representative compounds **4aa**, **4fa** and **4la** was determined by X-ray crystal diffraction, and we assigned the corresponding absolute configuration to all the obtained products. A large amount of experimental data suggested that the yields and enantioselectivities were close in value regardless of the *Z*/*E* configuration of the starting monofluoroalkenes. A full set of ^{19}F NMR tracking experiments was conducted, and these tracking experiments ultimately ruled out the possibility of *Z*/*E* isomerization of monofluoroalkenes (Supplementary Figs. 16–19).

Mechanistic considerations. Although we have developed a general method for enantioselective C(sp^3)–C(sp^3) bond formation, the reaction mechanism remains unclear. This reaction exhibited unusual regioselectivity that differed from that of hydrogen atom transfer reactions involving Co–H species[52–54]. Clarifying the stereo-determining step would be beneficial for developing additonal cobalt-catalysed asymmetric coupling reactions.

Our understanding of the reaction mechanism gradually improved with the help of a series of conventional experiments (Fig. 4). A set of radical clock experiments indicated a non-cage radical pathway for activating alkyl halides (Fig. 4a). When (bromomethyl)cyclopropane (**3G**) was subjected to standard conditions, a complex mixture of ring-opened products (**4aG**) was obtained; notably, the cyclopropyl ring was not retained (**4aG′**). 5-Iodopent-1-ene (**2H**) was subjected to the reaction, and we observed the cyclized product **4aH**. Moreover, the ratio of uncyclized (**4aH′**)/cyclized (**4aH**) products had a linear relationship with the concentration of cobalt catalyst. We used Ph_2SiD_2 to conduct deuterium-labelling experiments and studied the stereochemistry of this hydroalkylation reaction (Fig. 4b). We observed deuterium incorporation only at the β position of the fluorine substituent, and no H/D exchange was observed at the α position of either the fluorine or aryl substituents. The *Z*/*E* ratio of monofluoroalkene (**1d**) was correlated with the diastereoselectivity of deuterated monofluoroalkanes (d_1-**4dt** and d_1-**4dt′**). This reaction probably proceeded through an irreversible *syn*-hydrometalation of the Co–H intermediate across the monofluoroalkene in a highly regio- and enantioselective manner. Kinetic isotope effect experiments indicated that the hydrometalation step was the turnover-limiting step (Fig. 4c). The k_H/k_D value for Ph_2SiH_2 and Ph_2SiD_2 was found to be 1.76, revealing a primary kinetic deuterium isotope effect. In addition, the k_H/k_D value in the comparative experiments with **1a** and d_1-**1a** was 0.82, which was consistent with an inverse secondary kinetic deuterium isotope effect.

Next, we obtained more information about the cobalt catalyst (Fig. 4d). A linear relationship was observed between the enantiopurities of the ligand and the corresponding hydroalkylation product. Thus, the hydrometalation step might involve a monomeric cobalt complex bearing a single bisoxazoline ligand. In light of the ultraviolet–visible measurements and matrix-assisted laser desorption/ionization time-of-flight mass spectrometry (MALDI–TOF–MS) tests, we had sufficient evidence that CoX_2L^* (X = Br or I) was predominantly present in the reaction mixture and might represent the resting state of the catalyst. This reaction has a significant initiation period. We speculated that Co–H species were the actual catalytic species rather than the simple CoX_2L^*, which would require an additional initiation period to accomplish hydride transfer (Supplementary Fig. 23). We also evaluated the dependence of the average rate after the initiation period on the cobalt catalyst, monofluoroalkene, alkyl iodide and hydrosilane concentrations in each case. The model reaction exhibited a first-order dependence on the concentration of both the cobalt catalyst and monofluoroalkene and a zeroth-order dependence on the concentration of alkyl iodide and hydrosilane (Supplementary Figs. 24–31). These results revealed that the oxidation addition of alkyl iodide was a rapid and non-rate-determining step and that hydrometalation was the turnover-limiting step.

Density functional theory (DFT) calculations were first performed on a simplified reaction model. As shown in Fig. 5a, **q-[Co]BrH** is more stable than the doublet state **d-[Co]BrH** by 19.7 kcal mol^{-1}. However, the doublet migratory insertion step is kinetically more feasible, with the Gibbs free energy of the doublet transition state (TS) **d-TS1** being 8.3 kcal mol^{-1} lower than that of **q-TS1**. The pathway from **q-[Co]BrH** to **d-TS1** could significantly lower the overall activation barrier of the migratory insertion step. Given the different spin states of **q-[Co]BrH** (quartet) and **d-TS1** (doublet), spin crossover is involved in the reaction pathway, and was found to occur readily (Supplementary Fig. 34). Next, the four related TSs in the migratory insertion step were calculated. As shown, **d-TS1**, which leads to the major enantiomer and regioisomer product, has the lowest free energy (25.2 kcal mol^{-1}) compared to other competing TSs. After the migratory insertion step, the Co–alkyl product **d-Int1** undergoes oxidative addition with the alkyl radical to form **s-Int2** and **t-Int2**. Given the high energy of

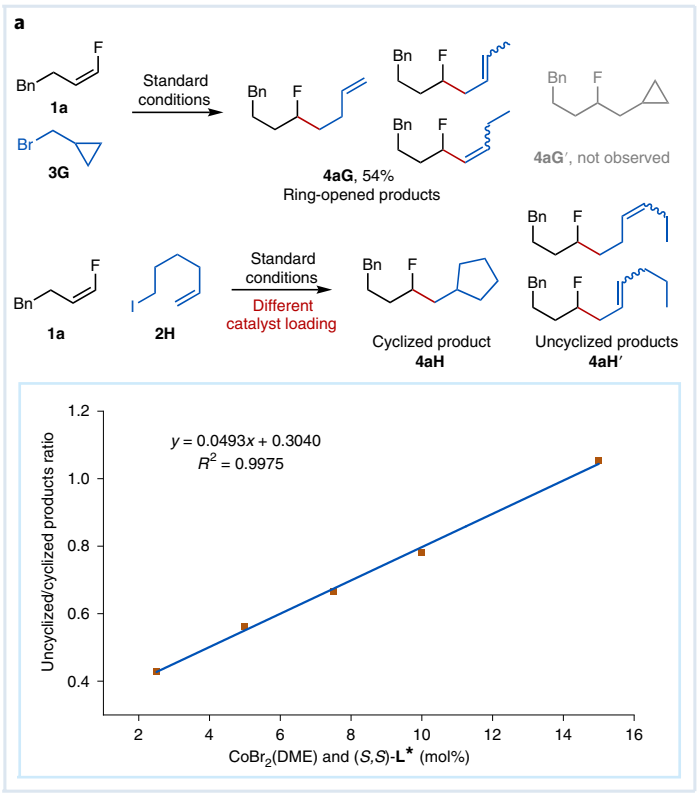

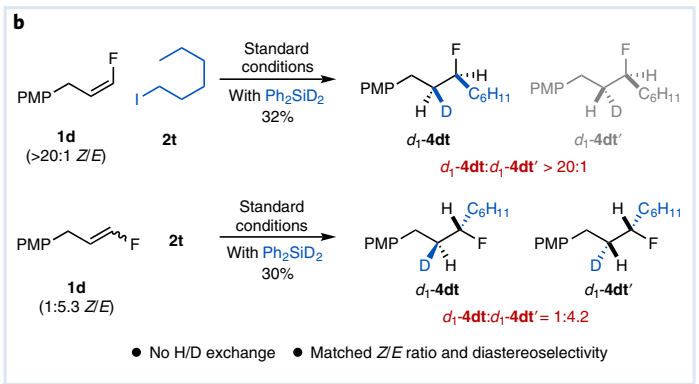

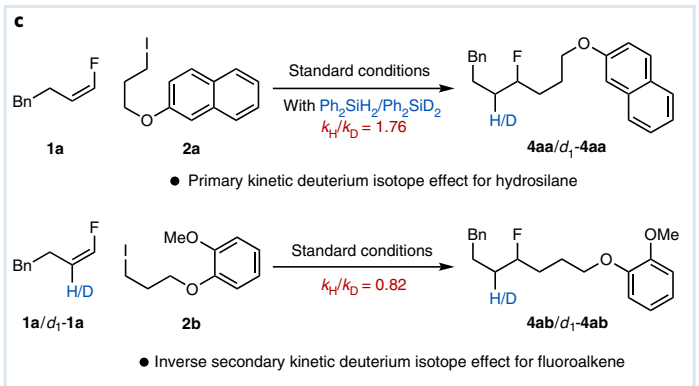

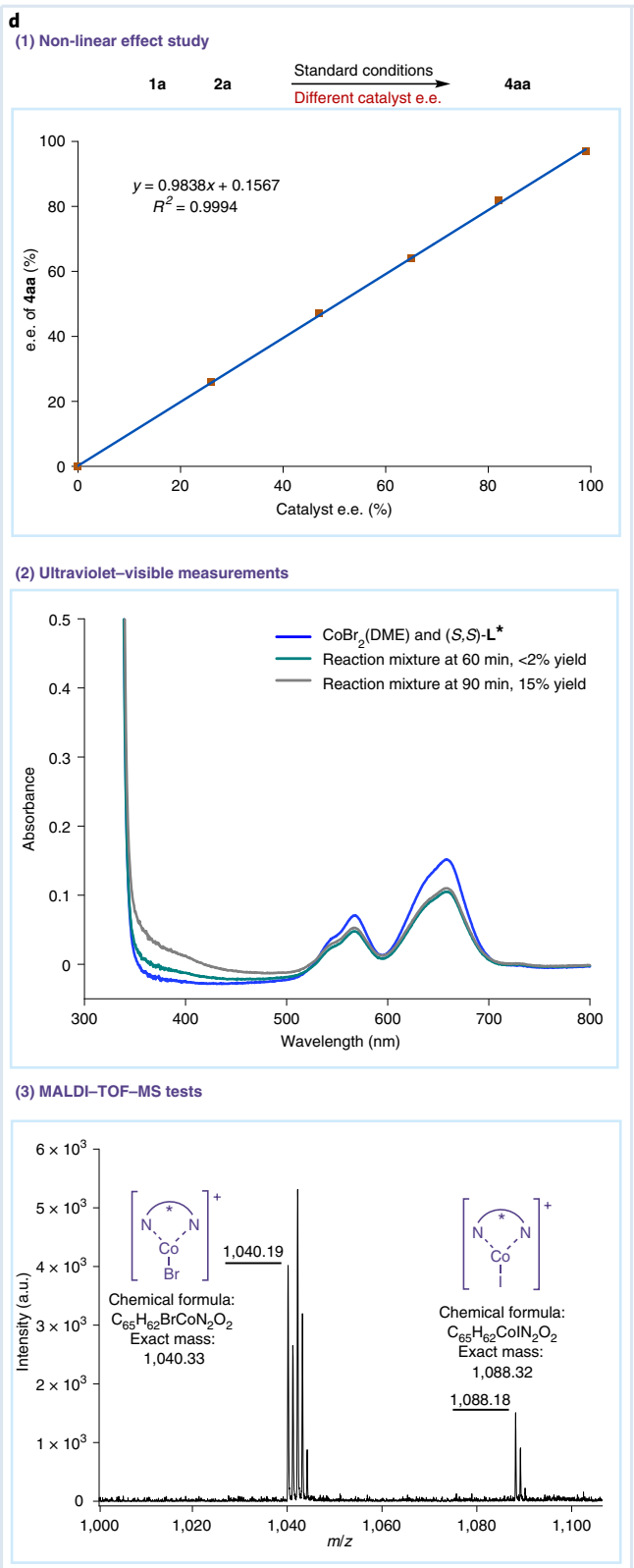

Fig. 4 | Preliminary mechanism studies. a, Radical clock experiments indicated alkyl halide activation through a non-cage radical pathway. **b**, Deuterium-labelling experiments indicated that *syn*-hydrometalation is the regio- and enantio-determining step. **c**, Kinetic isotope effect experiments indicated that *syn*-hydrometalation is the turnover-limiting step. In the reaction of **1a** and **2a** using Ph_2SiH_2 or Ph_2SiD_2, k_H is the reaction rate associated with Ph_2SiH_2, and k_D is the reaction rate associated with Ph_2SiD_2. In the reaction of **1a** or d_1-**1a** and **2b** under standard conditions, k_H is the reaction rate associated with **1a**, and k_D is the reaction rate associated with d_1-**1a**. **d**, Catalyst characterization using a non-linear effect study, ultraviolet–visible measurements, and MALDI-TOF-MS tests. The e.e. value was determined by HPLC. PMP, *p*-methoxyphenyl.

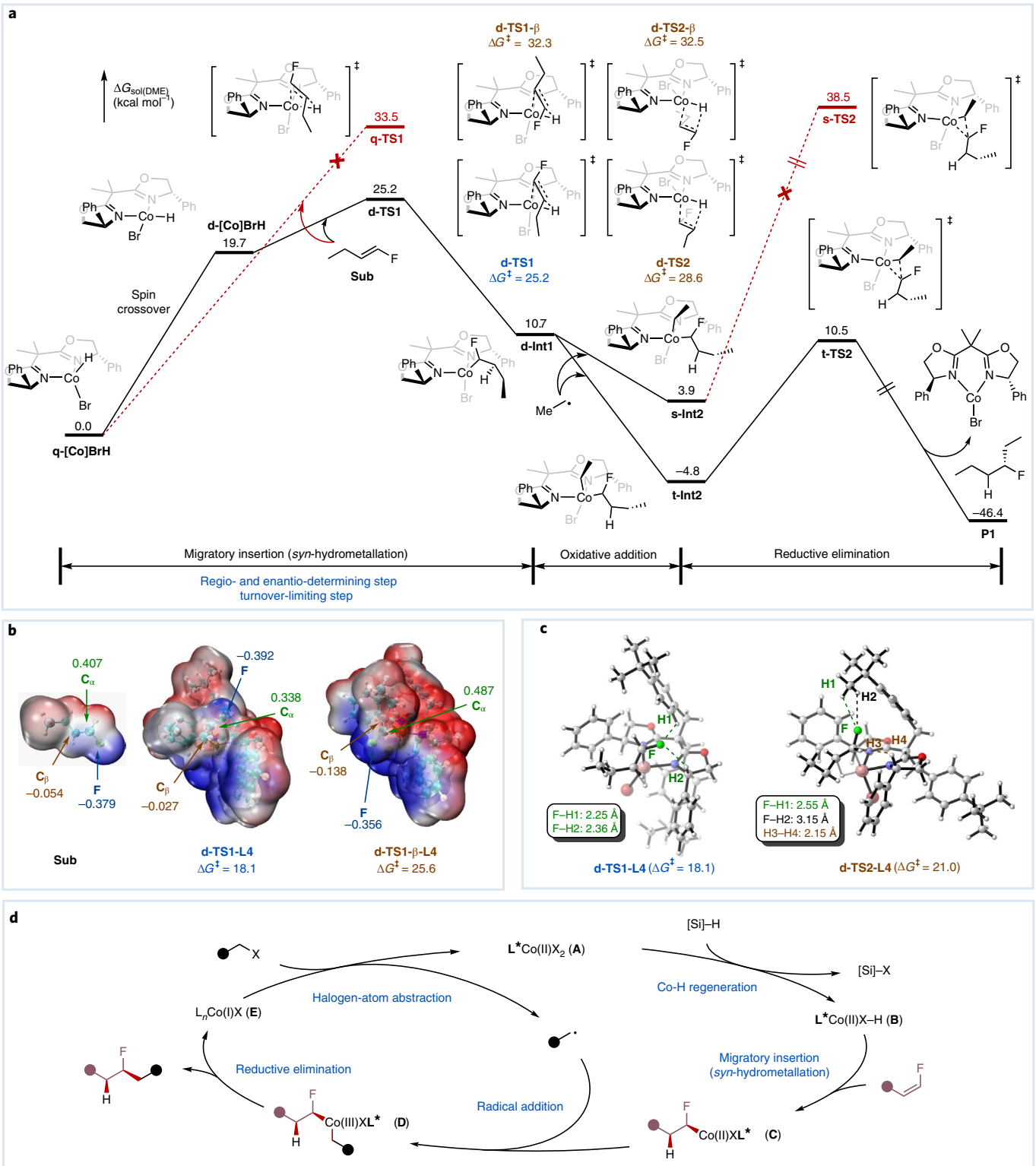

Fig. 5 | DFT calculations and proposed mechanism. a, DFT calculations at the B3LYP-D3(BJ)/6-311+G(d,p)-SDD-SMD(DME)//B3LYP-D3(BJ)/6-31G(d)-LANL2DZ level of theory. The prefixes s, d, t and q denote the singlet, doublet, triplet and quartet states of the examined species. Free energies are given in kcal mol^{-1}. **b**, Electronic effect analysis of the regio-determining step. NPA charges of the hydrogen atoms were added to those of the carbon atoms to which they were bound. **c**, Optimized structures of **d-TS1-L4** and **d-TS2-L4**. **d**, Proposed mechanism.

the reductive elimination transition state of **s-Int2**, that is, **s-TS2** (38.5 kcal mol^{-1}), the triplet pathway is more favourable for the reductive elimination. Throughout the catalytic cycle, the regio- and enantio-determining and turnover-limiting step was revealed as the migratory insertion step; a spin crossover for the cobalt catalyst was involved.

To further elucidate the origin of regio- and enantioselectivity, we computed the energy barriers of **d-TS1-L4**, **d-TS1-β-L4** and

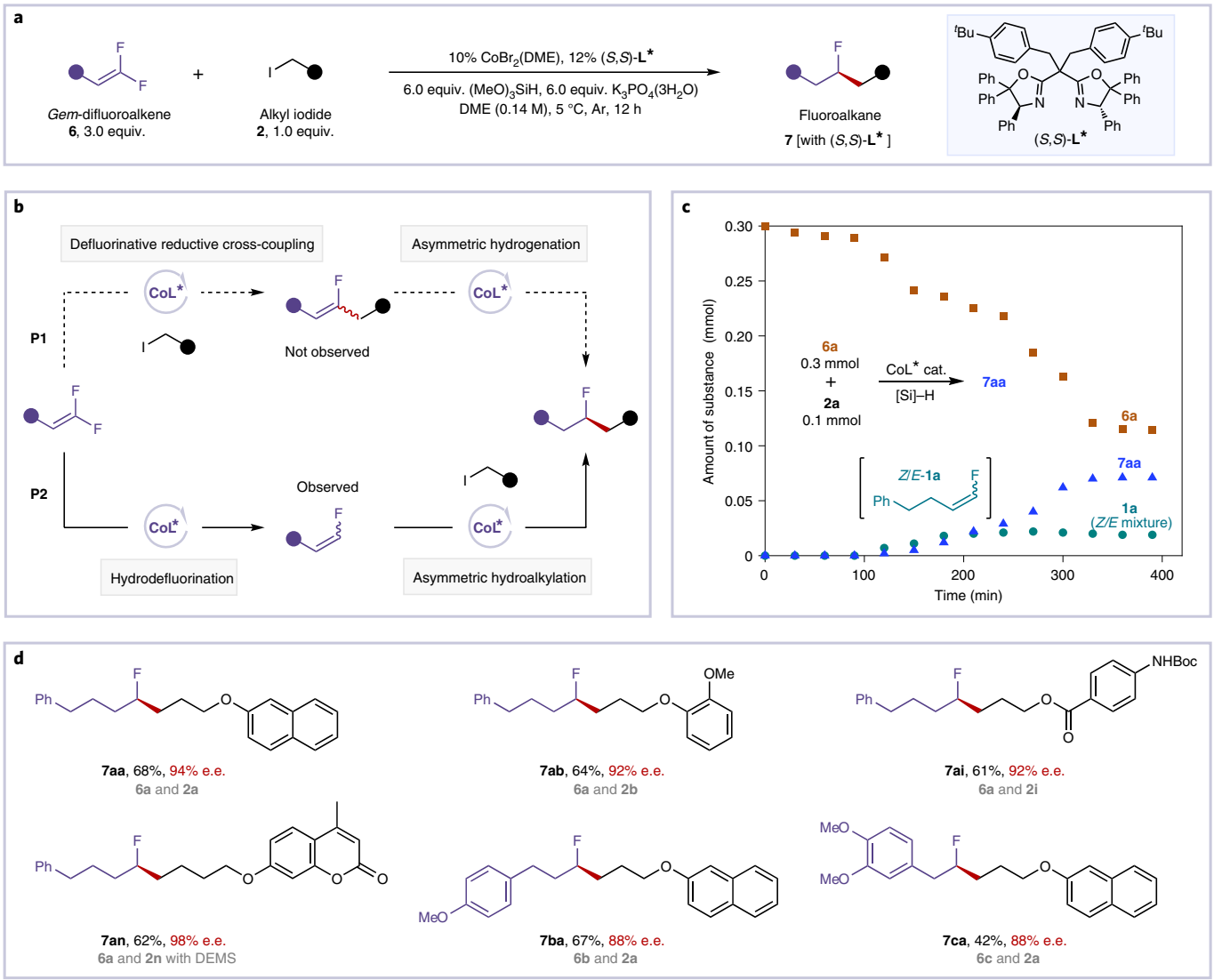

Fig. 6 | Defluorinative hydroalkylation. a, Reaction conditions for defluorinative hydroalkylation. **b**, Mechanistic hypothesis for defluorinative hydroalkylation. **c**, NMR tracking experiments indicated that the **P2** pathway is more reasonable. **d**, Substrate scope of defluorinative hydroalkylation. The e.e. value was determined by HPLC or SFC.

d-TS2-L4 with the experimentally used ligand **L4**. As shown in Fig. 5b, the high regioselectivity is manifested by the energy gap of 7.5 kcal mol^{-1} between **d-TS1-L4** and **d-TS1-β-L4**. The steric effect does not seem large enough to account for this significant energy gap, which led us to explore the electronic effects. The electrostatic potential on the 0.001 a.u. molecular surfaces of the **sub**, **d-TS1-L4** and **d-TS1-β-L4** and NPA charges on C_α, C_β and the fluorine atom **F** are shown in Fig. 5b. During the formation of Co–C bonds, the electron density on the C(H) of the substrate increases, that is, C_α: 0.407 (**sub**) → 0.338 (**d-TS1-L4**) and C_β: −0.054 (**sub**) → −0.138 (**d-TS1-β-L4**). Co–C bond formation in **d-TS1-L4** occurs between the cobalt and the α-fluorine carbon centre, and electron transfer to C_α is facilitated by the highly electronegative fluorine atom, resulting in the lower energy of **d-TS1-L4** than that of **d-TS1-β-L4**. Therefore, electronic effects dominate the regioselectivity. As shown in Fig. 5c, the relatively low Gibbs free energy of **d-TS1-L4** (18.1 kcal mol^{-1}) compared to that of **d-TS2-L4** (21.0 kcal mol^{-1}) can be attributed to the stronger non-covalent C–H···F interaction in **d-TS1-L4** and the destabilizing C–H···H–C repulsion in **d-TS2-L4**. In **d-TS1-L4**, the distances between the fluorine atom **F** of the substrate and the hydrogen atoms **H1** and **H2** of the ligand are shorter than the sum of their van der Waals radii (2.25 Å < 2.67 Å, 2.36 Å < 2.67 Å), suggesting the presence of stabilising C–H···F interactions. Although the C–H···F interaction is also present in **d-TS2-L4** (**F-H1**, 2.55 Å), it is weaker than that in **d-TS1-L4**. Moreover, in **d-TS2-L4**, the distance between the terminal vinyl hydrogen atom (**H3**) of the substrate and the hydrogen atom (**H4**) on the oxazoline of the ligand is shorter than the sum of their van der Waals radii (2.15 Å < 2.40 Å), indicating the presence of the destabilizing C–H···H–C repulsion in **d-TS2-L4**. Therefore, the enantioselectivity is attributed to both the stabilizing non-covalent interaction and destabilizing repulsion in different transition states.

Notably, a mechanistic variant involving Co(I)H for hydrometalation has also been proposed. However, the calculated regioselectivity in this pathway does not agree with the experimental data, making this variant involving Co(I)H species a relatively low-probability variant (Supplementary Table 8).

A presumptive mechanism for this cobalt-catalysed hydroalkylation was proposed (Fig. 5d). This proposed mechanism was similar to the radical chain mode in nickel chemistry[55,56]. The pivotal

steps include the generation of Co–H and its insertion into the C=C double bond, the formation and recombination of a non-cage alkyl radical, and finally the reductive elimination of a dialkyl Co(III) intermediate.

Defluorinative hydroalkylation. Finally, we applied cobalt-catalysed hydroalkylation conditions to a second family of substrates, *gem*-difluoroalkenes (Fig. 6). The *gem*-difluoroalkenes reacted with alkyl halides smoothly to produce chiral monofluoroalkanes under slightly modified conditions (Fig. 6a). The mechanistic hypothesis is outlined in Fig. 6b. In one of the proposed reaction pathways (**P1**), monofluoroalkenes were generated in the defluorinative reductive cross-coupling[57,58], and then asymmetric hydrogenation occurred to deliver the desired products. In an alternative pathway (**P2**), monofluoroalkanes were produced through hydrodefluorination and followed by asymmetric hydroalkylation. Since the monofluoroalkane intermediate **1a** was observed in NMR tracking experiments (Fig. 6c), this reaction probably proceeds through a defluorinative hydroalkylation pathway (**P2**). The substrate scope is summarized in Fig. 6d, and good coupling efficiency (42–68% yield) and high enantioinduction (88–98% e.e.) were obtained in all cases. A wide range of functional groups was well tolerated, such as ether (**7aa**, **7ab** and **7ba**), ester (**7ai**), carbamate (**7ai**) and coumarin heterocycle (**7an**). The aromatic substituted *gem*-difluoroalkene **6c** was also a suitable substrate in this defluorinative hydroalkylation.

Conclusions

We report a cobalt-catalysed enantioselective C(sp^3)–C(sp^3) coupling between readily available fluoroalkenes and alkyl halides. This reaction enables the streamlined synthesis of chiral fluoroalkanes with the introduction of an aliphatic C–F stereogenic centre at the desired position in an alkyl chain. This reaction exhibits a catalyst-controlled enantioselectivity, making traditional directing or auxiliary groups unnecessary. Preliminary mechanistic studies indicate that hydrometalation was the turnover-limiting step and stereo-determining step. This cobalt catalytic system may inspire the discovery of additional asymmetric coupling reactions.

Methods

General procedure for hydroalkylation. In air, a 10 ml screw-cap test tube equipped with a magnetic stirrer was charged with (*S*,*S*)-**L*** (0.024 mmol, 12 mol%), $CoBr_2$(DME) (0.02 mmol, 10 mol%) and CsF (0.6 mmol, 3.0 equiv.) (if the fluoroalkenes or the alkyl halides were solid, they were also added at this time). The test tube was evacuated and backfilled with argon three times. Then, DME (1.4 ml) was added, followed by the fluoroalkene (0.4 mmol, 2.0 equiv.) and alkyl halide (0.2 mmol, 1.0 equiv.). The resulting solution was stirred for 10 min at 0 °C. Then, DEMS (0.6 mmol, 3.0 equiv.) was added dropwise via a syringe, and the solution was stirred for 1 min at 0 °C, followed by stirring at 5 °C for 12 h. The reaction mixture was diluted with H_2O followed by extraction with EtOAc, dried with anhydrous Na_2SO_4 and concentrated in vacuo. The residue was purified by flash column chromatography on silica gel to obtain the target product.

General procedure for defluorinative hydroalkylation. In air, a 10 ml screw-cap test tube equipped with a magnetic stirrer was charged with (*S*,*S*)-**L*** (0.012 mmol, 12 mol%), $CoBr_2$(DME) (0.01 mmol, 10 mol%) and $K_3PO_4(3H_2O)$ (0.6 mmol, 6.0 equiv.) (if the fluoroalkenes or the alkyl halides were solid, they were also added at this time). The test tube was evacuated and backfilled with argon three times, and then DME (0.7 ml) was added, followed by the *gem*-difluoroalkene (0.3 mmol, 3.0 equiv.) and alkyl iodide (0.1 mmol, 1.0 equiv.). The resulting solution was stirred for 10 min at 0 °C. Then, $(MeO)_3SiH$ (0.6 mmol, 6.0 equiv.) was added dropwise via a syringe, and the solution was stirred for 1 min at 0 °C, followed by stirring at 5 °C for 12 h. The reaction mixture was diluted with H_2O followed by extraction with EtOAc, dried with anhydrous Na_2SO_4 and concentrated in vacuo. The residue was purified by flash column chromatography on silica gel to obtain the target product.

Data availability

Data supporting the findings of this study are available within the article and Supplementary Information files. The experimental procedures, characterization of the compounds and DFT calculations are available in the Supplementary Information. Crystallographic data for the structures reported in this article have been deposited at the Cambridge Crystallographic Data Centre, under deposition numbers CCDC 2055682 (**4aa**), 2088231 (**4fa**), and 2088232 (**4la**). Copies of the data can be obtained free of charge via https://www.ccdc.cam.ac.uk/structures/. All other data are available from the authors upon reasonable request.

Received: 7 February 2021; Accepted: 14 September 2021;
Published online: 20 October 2021

References

1. Geist, E., Kirschning, A. & Schmidt, T. sp^3–sp^3 coupling reactions in the synthesis of natural products and biologically active molecules. *Nat. Prod. Rep.* **31**, 441–448 (2014).
2. Lovering, F., Bikker, J. & Humblet, C. Escape from flatland: increasing saturation as an approach to improving clinical success. *J. Med. Chem.* **52**, 6752–6756 (2009).
3. Boström, J., Brown, D. G., Young, R. J. & Keserü, G. M. Expanding the medicinal chemistry synthetic toolbox. *Nat. Rev. Drug Discov.* **17**, 709–727 (2018).
4. Cherney, A. H., Kadunce, N. T. & Reisman, S. E. Enantioselective and enantiospecific transition-metal-catalyzed cross-coupling reactions of organometallic reagents to construct C–C bonds. *Chem. Rev.* **115**, 9587–9652 (2015).
5. Choi, J. & Fu, G. C. Transition metal-catalyzed alkyl–alkyl bond formation: another dimension in cross-coupling chemistry. *Science* **356**, eaaf7230 (2017).
6. Tasker, S. Z., Standley, E. A. & Jamison, T. F. Recent advances in homogeneous nickel catalysis. *Nature* **509**, 299–309 (2014).
7. Yin, H. & Fu, G. C. Mechanistic investigation of enantioconvergent Kumada reactions of racemic α-bromoketones catalyzed by a nickel/bis(oxazoline) complex. *J. Am. Chem. Soc.* **141**, 15433–15440 (2019).
8. Fu, G. C. Transition-metal catalysis of nucleophilic substitution reactions: a radical alternative to S_N1 and S_N2 processes. *ACS Cent. Sci.* **3**, 692–700 (2017).
9. Schwarzwalder, G. M., Matier, C. D. & Fu, G. C. Enantioconvergent cross-couplings of alkyl electrophiles: the catalytic asymmetric synthesis of organosilanes. *Angew. Chem. Int. Ed.* **58**, 3571–3574 (2019).
10. Liang, Y. & Fu, G. C. Stereoconvergent Negishi arylations of racemic secondary alkyl electrophiles: differentiating between a CF_3 and an alkyl group. *J. Am. Chem. Soc.* **137**, 9523–9526 (2015).
11. Lu, Z., Wilsily, A. & Fu, G. C. Stereoconvergent amine-directed alkyl–alkyl Suzuki reactions of unactivated secondary alkyl chlorides. *J. Am. Chem. Soc.* **133**, 8154–8157 (2011).
12. Huo, H., Gorsline, B. J. & Fu, G. C. Catalyst-controlled doubly enantioconvergent coupling of racemic alkyl nucleophiles and electrophiles. *Science* **367**, 559–564 (2020).
13. Kadunce, N. T. & Reisman, S. E. Nickel-catalyzed asymmetric reductive cross-coupling between heteroaryl iodides and α-chloronitriles. *J. Am. Chem. Soc.* **137**, 10480–10483 (2015).
14. Schmidt, J., Choi, J., Liu, A. T., Slusarczyk, M. & Fu, G. C. A general, modular method for the catalytic asymmetric synthesis of alkylboronate esters. *Science* **354**, 1265–1269 (2016).
15. Wang, X.-X., Lu, X., Li, Y., Wang, J.-W. & Fu, Y. Recent advances in nickel-catalyzed reductive hydroalkylation and hydroarylation of electronically unbiased alkenes. *Sci. China Chem.* **63**, 1586–1600 (2020).
16. Lu, X. et al. Practical carbon–carbon bond formation from olefins through nickel-catalyzed reductive olefin hydrocarbonation. *Nat. Commun.* **7**, 11129 (2016).
17. Lu, X., Xiao, B., Liu, L. & Fu, Y. Formation of C(sp^3)–C(sp^3) bonds through nickel-catalyzed decarboxylative olefin hydroalkylation reactions. *Chem. Eur. J.* **22**, 11161–11164 (2016).
18. Wang, Z., Yin, H. & Fu, G. C. Catalytic enantioconvergent coupling of secondary and tertiary electrophiles with olefins. *Nature* **563**, 379–383 (2018).
19. Zhou, F., Zhang, Y., Xu, X. & Zhu, S. NiH-catalyzed remote asymmetric hydroalkylation of alkenes with racemic α-bromo amides. *Angew. Chem. Int. Ed.* **58**, 1754–1758 (2019).
20. He, S.-J. et al. Nickel-catalyzed enantioconvergent reductive hydroalkylation of olefins with α-heteroatom phosphorus or sulfur alkyl electrophiles. *J. Am. Chem. Soc.* **142**, 214–221 (2020).
21. Miki, Y., Hirano, K., Satoh, T. & Miura, M. Copper-catalyzed intermolecular regioselective hydroamination of styrenes with polymethylhydrosiloxane and hydroxylamines. *Angew. Chem. Int. Ed.* **52**, 10830–10834 (2013).
22. Shi, S.-L., Wong, Z. L. & Buchwald, S. L. Copper-catalysed enantioselective stereodivergent synthesis of amino alcohols. *Nature* **532**, 353–356 (2016).
23. Wang, Y.-M., Bruno, N. C., Placeres, Á. L., Zhu, S. & Buchwald, S. L. Enantioselective synthesis of carbo- and heterocycles through a CuH-catalyzed hydroalkylation approach. *J. Am. Chem. Soc.* **137**, 10524–10527 (2015).
24. Liu, R. Y. & Buchwald, S. L. CuH-catalyzed olefin functionalization: from hydroamination to carbonyl addition. *Acc. Chem. Res.* **53**, 1229–1243 (2020).

25. Bera, S., Mao, R. & Hu, X. Enantioselective C(sp^3)–C(sp^3) cross-coupling of non-activated alkyl electrophiles via nickel hydride catalysis. *Nat. Chem.* **13**, 270–277 (2021).
26. Wang, J.-W. et al. Catalytic asymmetric reductive hydroalkylation of enamides and enecarbamates to chiral aliphatic amines. *Nat. Commun.* **12**, 1313 (2021).
27. He, Y., Liu, C., Yu, L. & Zhu, S. Enantio- and regioselective NiH-catalyzed reductive hydroarylation of vinylarenes with aryl iodides. *Angew. Chem. Int. Ed.* **59**, 21530–21534 (2020).
28. Qian, D., Bera, S. & Hu, X. Chiral alkyl amine synthesis via catalytic enantioselective hydroalkylation of enecarbamates. *J. Am. Chem. Soc.* **143**, 1959–1967 (2021).
29. Shi, L., Xing, L.-L., Hu, W.-B. & Shu, W. Regio- and enantioselective Ni-catalyzed formal hydroalkylation, hydrobenzylation, and hydropropargylation of acrylamides to α-tertiary amides. *Angew. Chem. Int. Ed.* **60**, 1599–1604 (2021).
30. Wang, X.-X. et al. NiH-catalyzed reductive hydrocarbonation of enol esters and ethers. *CCS Chem.* **3**, 727–737 (2021).
31. Hapke, M. & Hilt, G. in *Cobalt Catalysis in Organic Synthesis* (eds Hapke, M. & Hilt, G.) 1–23 (Wiley-VCH, 2020).
32. Hammann, J. M., Hofmayer, M. S., Lutter, F. H., Thomas, L. & Knochel, P. Recent advances in cobalt-catalyzed Csp^2 and Csp^3 cross-couplings. *Synthesis* **49**, 3887–3894 (2017).
33. Rérat, A. & Gosmini, C. Grignard reagents and cobalt. *Phys. Sci. Rev.* **3**, 20160021 (2018).
34. Dorval, C. & Gosmini, C. in *Cobalt Catalysis in Organic Synthesis* (eds Hapke, M. & Hilt, G.) 163–205 (Wiley-VCH, 2020).
35. Pellissier, H. Recent developments in enantioselective cobalt-catalyzed transformations. *Coord. Chem. Rev.* **360**, 122–168 (2018).
36. Pellissier, H. in *Cobalt Catalysis in Organic Synthesis* (eds Hapke, M. & Hilt, G.) 337–416 (Wiley-VCH, 2020).
37. Mao, J. et al. Cobalt–bisoxazoline-catalyzed asymmetric Kumada cross-coupling of racemic α-bromo esters with aryl Grignard reagents. *J. Am. Chem. Soc.* **136**, 17662–17668 (2014).
38. Ni, C. & Hu, J. The unique fluorine effects in organic reactions: recent facts and insights into fluoroalkylations. *Chem. Soc. Rev.* **45**, 5441–5454 (2016).
39. Moschner, J. et al. Approaches to obtaining fluorinated α-amino acids. *Chem. Rev.* **119**, 10718–10801 (2019).
40. Sladojevich, F., Arlow, S. I., Tang, P. & Ritter, T. Late-stage deoxyfluorination of alcohols with phenofluor. *J. Am. Chem. Soc.* **135**, 2470–2473 (2013).
41. He, Y., Yang, Z., Thornbury, R. T. & Toste, F. D. Palladium-catalyzed enantioselective 1,1-fluoroarylation of aminoalkenes. *J. Am. Chem. Soc.* **137**, 12207–12210 (2015).
42. Jiang, X. & Gandelman, M. Enantioselective Suzuki cross-couplings of unactivated 1-fluoro-1-haloalkanes: synthesis of chiral β-, γ-, δ-, and ε-fluoroalkanes. *J. Am. Chem. Soc.* **137**, 2542–2547 (2015).
43. Yang, X., Wu, T., Phipps, R. J. & Toste, F. D. Advances in catalytic enantioselective fluorination, mono-, di-, and trifluoromethylation, and trifluoromethylthiolation reactions. *Chem. Rev.* **115**, 826–870 (2015).
44. Nielsen, M. K., Ahneman, D. T., Riera, O. & Doyle, A. G. Deoxyfluorination with sulfonyl fluorides: navigating reaction space with machine learning. *J. Am. Chem. Soc.* **140**, 5004–5008 (2018).
45. Zhu, Y. et al. Modern approaches for asymmetric construction of carbon–fluorine quaternary stereogenic centers: synthetic challenges and pharmaceutical needs. *Chem. Rev.* **118**, 3887–3964 (2018).
46. Liu, J., Yuan, Q., Toste, F. D. & Sigman, M. S. Enantioselective construction of remote tertiary carbon–fluorine bonds. *Nat. Chem.* **11**, 710–715 (2019).
47. Huang, W., Wan, X. & Shen, Q. Cobalt-catalyzed asymmetric cross-coupling reaction of fluorinated secondary benzyl bromides with lithium aryl boronates/$ZnBr_2$. *Org. Lett.* **22**, 4327–4332 (2020).
48. Cox, D. G., Gurusamy, N. & Burton, D. J. Surprising stereochemical control of Wittig olefination involving reaction of fluorine-containing phosphoranium salt and aldehydes. *J. Am. Chem. Soc.* **107**, 2811–2812 (1985).
49. Koh, M. J., Nguyen, T. T., Zhang, H., Schrock, R. R. & Hoveyda, A. H. Direct synthesis of *Z*-alkenyl halides through catalytic cross-metathesis. *Nature* **531**, 459–465 (2016).
50. Jiang, X., Sakthivel, S., Kulbitski, K., Nisnevich, G. & Gandelman, M. Efficient synthesis of secondary alkyl fluorides via Suzuki cross-coupling reaction of 1-halo-1-fluoroalkanes. *J. Am. Chem. Soc.* **136**, 9548–9551 (2014).
51. Abad, J.-L., Villorbina, G., Fabriàs, G. & Camps, F. Synthesis of fluorinated analogs of myristic acid as potential inhibitors of Egyptian armyworm (*Spodoptera littorialis*) Δ^{11} desaturasedesaturase. *Lipids* **38**, 865–871 (2003).
52. Waser, J. & Carreira, E. M. Convenient synthesis of alkylhydrazides by the cobalt-catalyzed hydrohydrazination reaction of olefins and azodicarboxylates. *J. Am. Chem. Soc.* **126**, 5676–5677 (2004).
53. Crossley, S. W., Obradors, C., Martinez, R. M. & Shenvi, R. A. Mn-, Fe-, and Co-catalyzed radical hydrofunctionalizations of olefins. *Chem. Rev.* **116**, 8912–9000 (2016).
54. Ai, W., Zhong, R., Liu, X. & Liu, Q. Hydride transfer reactions catalyzed by cobalt complexes. *Chem. Rev.* **119**, 2876–2953 (2019).
55. Biswas, S. & Weix, D. J. Mechanism and selectivity in nickel-catalyzed cross-electrophile coupling of aryl halides with alkyl halides. *J. Am. Chem. Soc.* **135**, 16192–16197 (2013).
56. Schley, N. D. & Fu, G. C. Nickel-catalyzed Negishi arylations of propargylic bromides: a mechanistic investigation. *J. Am. Chem. Soc.* **136**, 16588–16593 (2014).
57. Lu, X. et al. Nickel-catalyzed allylic defluorinative alkylation of trifluoromethyl alkenes with reductive decarboxylation of redox-active esters. *Chem. Sci.* **10**, 809–814 (2019).
58. Lu, X. et al. Nickel-catalyzed defluorinative reductive cross-coupling of *gem*-difluoroalkenes with unactivated secondary and tertiary alkyl halides. *J. Am. Chem. Soc.* **139**, 12632–12637 (2017).

Acknowledgements

Financial support from the National Natural Science Foundation of China (grant numbers 21732006, 51821006 and 51961135104 for Y.F. and grant number 21927814 for X.L.) and the USTC Research Funds of the Double First-Class Initiative (grant number YD3530002002 for X.L.) is acknowledged. We thank L. Yu (HMFL) and C.L. Tian (USTC) for helpful discussions.

Author contributions

X.L. and Y.F. directed the project and wrote the manuscript with input from all other authors. Y.F. directed and W.N. performed the DFT calculations. Under the guidance of X.L., Y.L. developed the methods, and Y.L. and J.-W.W. designed and performed the synthetic and mechanistic experiments with the help of Z.C. All the authors participated in the discussion and preparation of the manuscript.

Competing interests

The authors declare no competing interests.

Additional information

Supplementary information The online version contains supplementary material available at https://doi.org/10.1038/s41929-021-00688-w.

Correspondence and requests for materials should be addressed to Xi Lu or Yao Fu.

Peer review information *Nature Catalysis* thanks Corinne Gosmini and the other, anonymous, reviewer(s) for their contribution to the peer review of this work.

Reprints and permissions information is available at www.nature.com/reprints.

Publisher's note Springer Nature remains neutral with regard to jurisdictional claims in published maps and institutional affiliations.